metals

MDPI

Article

Effect of Substrate Temperature on Bead Track Geometry of 316L in Directed Energy Deposition: Investigation and Regression Modeling

Deviprasad Chalicheemalapalli Jayasankar *, Stefan Gnaase, Dennis Lehnert, Artur Walter, Robin Rohling and Thomas Tröster

Institute for Lightweight Design with Hybrid Systems (ILH), Automotive Lightweight Design (LiA), Paderborn University, Warburger Str. 100, 33098 Paderborn, Germany; stefan.gnaase@uni-paderborn.de (S.G.); dennis.lehnert@uni-paderborn.de (D.L.); arturw@campus.uni-paderborn.de (A.W.); rohling@campus.uni-paderborn.de (R.R.); thomas.troester@upb.de (T.T.)

* Correspondence: deviprasad.jayasankar@uni-paderborn.de

Abstract: The optimization of process parameters in powder Directed Energy Deposition (DED) is essential for achieving consistent, high-quality bead geometries, which directly influence the performance and structural integrity of fabricated components. As a subset of additive manufacturing (AM), the DED process, also referred to as laser metal deposition (LMD), enables precise, layer-by-layer material deposition, making it highly suitable for complex geometries and part repair applications. Critical parameters, such as the laser power, feed rate, powder mass flow, and substrate temperature govern the deposition process, impacting the bead height, width, contact angle, and dilution. Inconsistent control over these variables can lead to defects, such as poor bonding, dimensional inaccuracies, and material weaknesses, ultimately compromising the final product. This paper investigates the effects of various process parameters, specifically the substrate temperature, on bead track geometry in DED processes for stainless steel (1.4404). A specialized experimental setup, integrated within a DED machine, facilitates the controlled thermal conditioning of sample sheets. Using Design of Experiments (DoE) methods, individual bead marks are generated and analyzed to assess geometric characteristics. Regression models, including both linear and quadratic approaches, are constructed to predict machine parameters for achieving the desired bead geometry at different substrate temperatures. Validation experiments confirm the accuracy and reliability of the models, particularly in predicting the bead height, bead width, and contact angle across a broad range of substrate temperatures. However, the models demonstrated limitations in accurately predicting dilution, indicating the need for further refinement. Despite some deviations in measured values, successful fabrication is achieved, demonstrating robust bonding between the bead and substrate. The developed models offer insights into optimizing DED process parameters to achieve desired bead characteristics, advancing the precision and reliability of additive manufacturing technology. Future work will focus on refining the regression models to improve predictions, particularly for dilution, and further investigate non-linear interactions between process variables.

Keywords: additive manufacturing (AM); direct energy deposition (DED); laser metal deposition (LMD); AISI 316L austenitic stainless steel (1.4404)

Citation: Chalicheemalapalli Jayasankar, D.; Gnaase, S.; Lehnert, D.; Walter, A.; Rohling, R.; Tröster, T. Effect of Substrate Temperature on Bead Track Geometry of 316L in Directed Energy Deposition: Investigation and Regression Modeling. *Metals* **2024**, *14*, 1353. https://doi.org/10.3390/met14121353

Received: 16 October 2024
Revised: 14 November 2024
Accepted: 25 November 2024
Published: 27 November 2024

1. Introduction

In the rapidly evolving field of additive manufacturing (AM), optimizing process parameters is essential for producing components with the required structural integrity and functional performance [1,2]. AM technologies allow for the creation of complex geometries layer by layer, making them suitable for industries, such as aerospace, automotive, and tooling [3,4]. Among these technologies, Directed Energy Deposition (DED) has gained significant attention due to its versatility in fabricating new parts, repairing

high-value components, and producing functionally graded materials [5,6]. While electron beam-based DED can provide high energy for certain applications, it requires a vacuum environment, which is generally impractical for most robotized cells due to the added complexity and equipment cost. DED processes are broadly classified based on the energy source used—such as laser (DED-LB), electron beam, or plasma arc—and the form of material, either powder or wire. Each DED process family offers unique advantages depending on the application requirements and operational environment. This paper focuses on powder-based DED-LB, which, despite some drawbacks, offers a competitive advantage in terms of precision and the surface finish as shown in Figure 1. Powder DED-LB systems are particularly advantageous for applications requiring high control over deposition rates and intricate geometries due to the focused laser energy. Although powder-based systems may have limitations regarding material utilization and cost, their ability to produce fine, detailed structures makes them suitable for high-value applications in aerospace, automotive, and medical fields, where accuracy and complex geometries are critical [7–9].

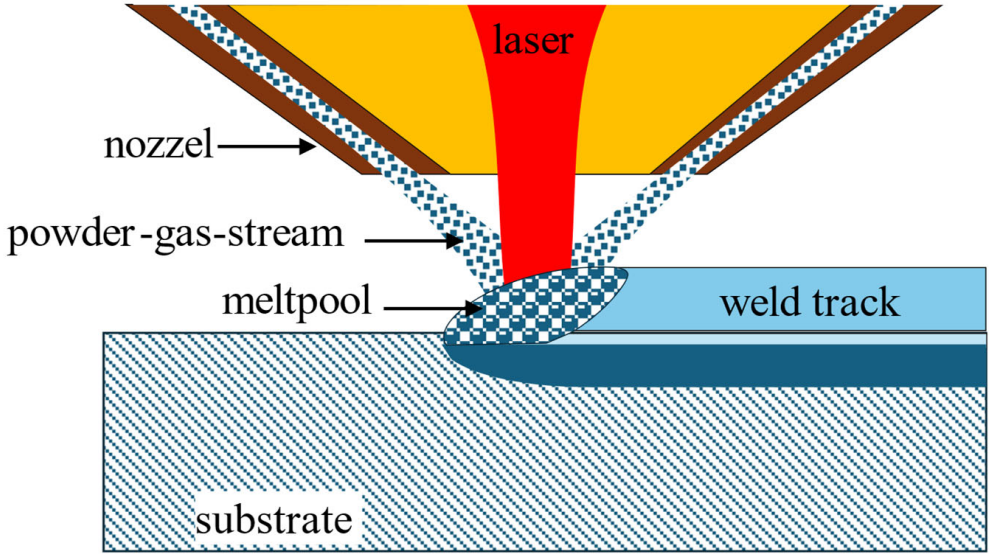

Figure 1. Schematics of the DED-LB process.

Recent advances in DED-LB process optimization have focused on critical parameters, such as the laser power, powder feed rate, traverse speed (feed rate), contact angle, and substrate temperature [10–12]. These factors play crucial roles in determining bead track geometry and ultimately the quality of the final component [13–15]. For instance, laser power governs the melt pool dimensions and energy input, directly influencing the bead depth and width. Research shows that increasing the laser power, typically in the range of 500 W to 3000 W, can enhance the penetration depth, but excessive power can result in keyholing or vaporization if not balanced with other factors [16,17]. Similarly, the feed rate, which controls the deposition speed, affects layer formation, with slower feed rates (e.g., 200 mm/min to 1200 mm/min) resulting in wider and deeper bead pools, but also increasing the heat-affected zone (HAZ) [18]. Higher feed rates can reduce bonding strength by limiting the energy input, potentially leading to insufficient fusion.

The contact angle also plays a significant role in ensuring proper interlayer fusion and minimizing defects, like porosity or cracking. Maintaining contact angles between 120° and 140° has been shown to promote strong interlayer bonding, whereas deviations can lead to poor adhesion and structural weakness [19,20]. The substrate temperature, another critical factor, influences the cooling rate and thermal gradients, which affect residual stress and the microstructure. Preheating the substrate to temperatures between 200 °C and 800 °C has been found to reduce thermal stresses and improve metallurgical bonding between layers, though excessively high temperatures can lead to undesirable microstructural changes [11].

In addition to these key parameters, the powder flow rate, laser spot size, and scanning pattern are known to impact DED-LB outcomes [21]. For instance, the powder flow rate influences the deposition efficiency and layer homogeneity, with excessive flow rates causing uneven layers, while too little powder results in weak bonding. The laser spot size affects energy distribution in the melt pool, with larger spots promoting uniform energy input but reducing the resolution. Conversely, smaller spot sizes offer precision but risk localized overheating. The scanning pattern, dictating the laser path, affects the heat distribution and residual stress, with improper patterns leading to warping or distortion.

Although many factors influence DED-LB, in this study, a regression model was formulated based on the laser power, feed rate, contact angle, and substrate temperature, focusing on their direct influence on bead geometry for single bead tracks. These four parameters govern key aspects of the process, such as energy input and layer adhesion, making their optimization critical to achieving dimensional accuracy and high-quality part production. To systematically explore the interactions between these variables, we employed a full factorial Design of Experiments (DoE), which tests all possible combinations of selected parameters and their levels. This approach ensures that both main effects and interaction effects are thoroughly evaluated, providing a comprehensive understanding of how each parameter influences bead geometry [22,23]. Following the experiments, the Pearson correlation coefficient was applied to quantify the linear relationships between process variables and bead characteristics. The Pearson correlation coefficient ranges from -1 to 1, with values close to 1 indicating strong positive correlations and values near -1 indicating strong negative correlations. This analysis helped prioritize variables with the most significant impact on bead geometry, guiding further optimization efforts.

By combining full factorial DoE with Pearson correlation analysis, we developed a regression equation for identifying critical factors in DED-LB processes [24]. This approach helps optimize parameters that influence bead characteristics for improved structural integrity and performance.

2. Materials and Methods

2.1. Material Selection

In DED-LB processes, materials are chosen based on the specific application requirements. In this study, 1.4404 (AISI 316L) stainless steel was selected as the experimental material (Tables 1 and 2), due to its excellent corrosion resistance, mechanical stability, and suitability for high-temperature applications. Its low carbon content reduces carbide precipitation during deposition, minimizing the risk of intergranular corrosion and thus preserving structural integrity. Additionally, 1.4404 demonstrates stable mechanical performance through repeated heating and cooling cycles, making it ideal for processes requiring precise bead geometry control. This material was chosen over alternatives for its versatility, ease of processing in standard DED-LB setups, and reliable performance in additive manufacturing, ensuring reproducibility, a reduced defect risk, and a balance of mechanical properties with corrosion resistance.

Table 1. Mechanical properties of the 1.4404 (AISI 316L) stainless steel.

Tensile Strength/MPa	Yield Strength/MPa	Elongation at Break/%	Hardness/HV10	Surface Roughness/Ra
605	550	45	215	6

Table 2. Chemical composition of AISI 316L (wt.%).

Cr	Ni	Mo	Mn	Si	C	Fe
16.8	11.9	2.5	1.3	0.3	0.01	Balance

2.2. Sample Production

For the sample production, a heating system was integrated into the workspace of the DMG MORI LT65 3D DED machine. This setup included a ceramic holder to secure the sample sheets and provide insulation and electrical isolation as shown in Figure 2.

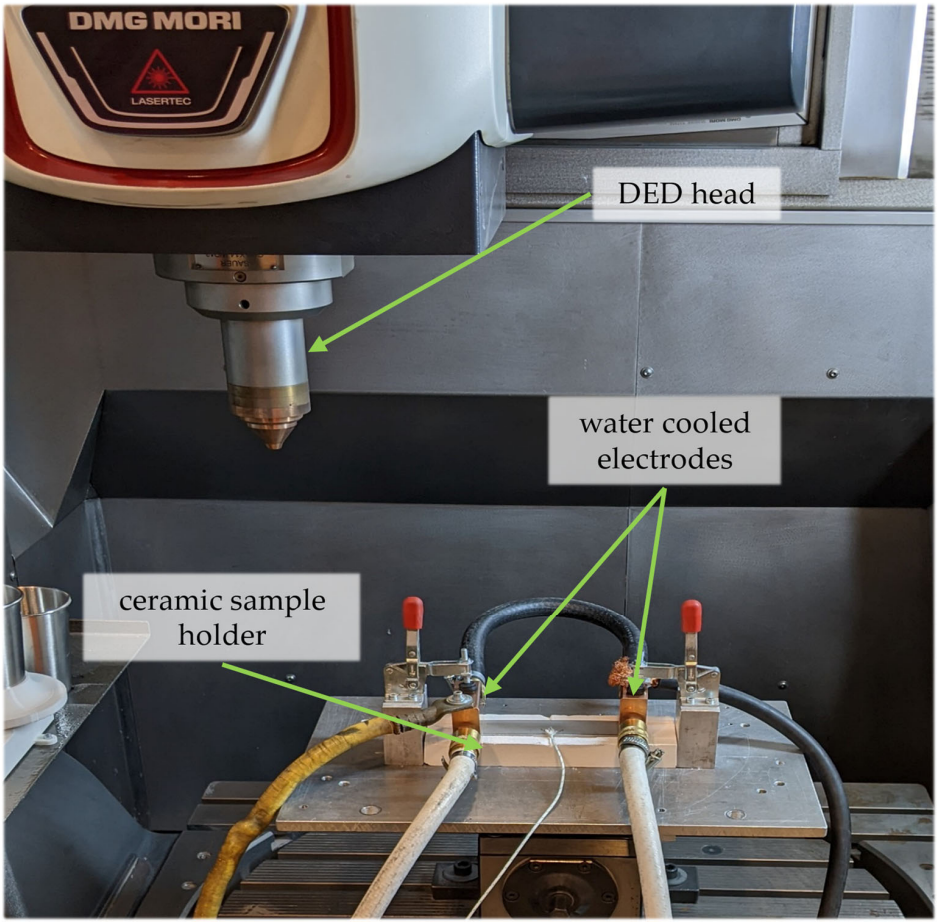

Figure 2. Sample production setup.

It should be noted that the experimental setup in this study was specifically configured for the DMG MORI LT65 3D DED machine (DMG MORI Academy GmbH, Bielefeld, Germany). However, with minor adjustments, the same setup principles can be applied to other DED platforms with comparable capabilities. The sample sheets were made of 1.4404 stainless steel and measured 30 × 170 × 3 mm. They were attached to the holder using water-cooled electrodes. A welding transformer delivered a peak current of 630 A at 4.85 V to heat the sheets. The temperature was monitored with an infrared camera (Optris Pl400i—Optris GmbH, Berlin, Germany) and thermocouples. The standard COAX14 AA13 nozzle (DMG MORI Academy GmbH, Bielefeld, Germany) was used for powder delivery. The experiment began by positioning the laser head at the start point, and the feed rate was initially set to 0%. The sample sheets were heated to 50 °C above the target temperature, and once the temperature was within ±5 °C of the target, the feed rate was restored to 100%, and the cladding began. Five individual bead tracks, each 20 mm in length, were deposited onto the heated substrate under the same powder mass flow rate. The process parameters were varied as shown in Table 3. Laser power values of 500, 1000, 1500, 2000, and 2500 W were chosen to examine a broad range of energy inputs, which influence the size and shape of the melt pool and affect the bead width, height, and fusion characteristics. Similarly, traverse speeds of 400, 800, and 1200 mm/min were selected to evaluate the effects of varying deposition rates on bead geometry and to identify optimal feed rates

for achieving consistent layer deposition. Powder mass flow rates were set at 5, 12.5, and 20 g/min, allowing us to explore different material delivery rates, which influence the layer thickness, bonding quality, and deposition efficiency. By controlling the powder mass flow, we aimed to maintain a stable deposition process while achieving consistent bead characteristics. Substrate temperature values, ranging from room temperature (RT) up to 1000 °C, were chosen to investigate how thermal conditions influence material flow, bonding, and microstructure development in the deposited material. This range covers a variety of preheating scenarios, from ambient temperature to significantly elevated temperatures, allowing us to observe how thermal gradients and cooling rates affect key geometric characteristics, such as the bead width, height, contact angle, and dilution.

Table 3. Experimental parameters for sample production.

Parameter	Values
Laser Power (W)	■ 500 ■ 1000 ■ 1500 ■ 2000 ■ 2500
Traverse Speed (mm/min)	■ 400 ■ 800 ■ 1200
Powder Mass Flow (g/min)	■ 5 ■ 12.5 ■ 20
Substrate Temperature (°C)	■ RT ■ 100 ■ 200 ■ 300 ■ 400 ■ 600 ■ 800 ■ 1000

Overall, these parameter ranges were selected to provide a comprehensive understanding of their influence on DED outcomes, enabling the development of predictive models for optimized process conditions. A total of 325 bead tracks were produced as shown in Figure 3. The samples were labeled accordingly and prepared for testing.

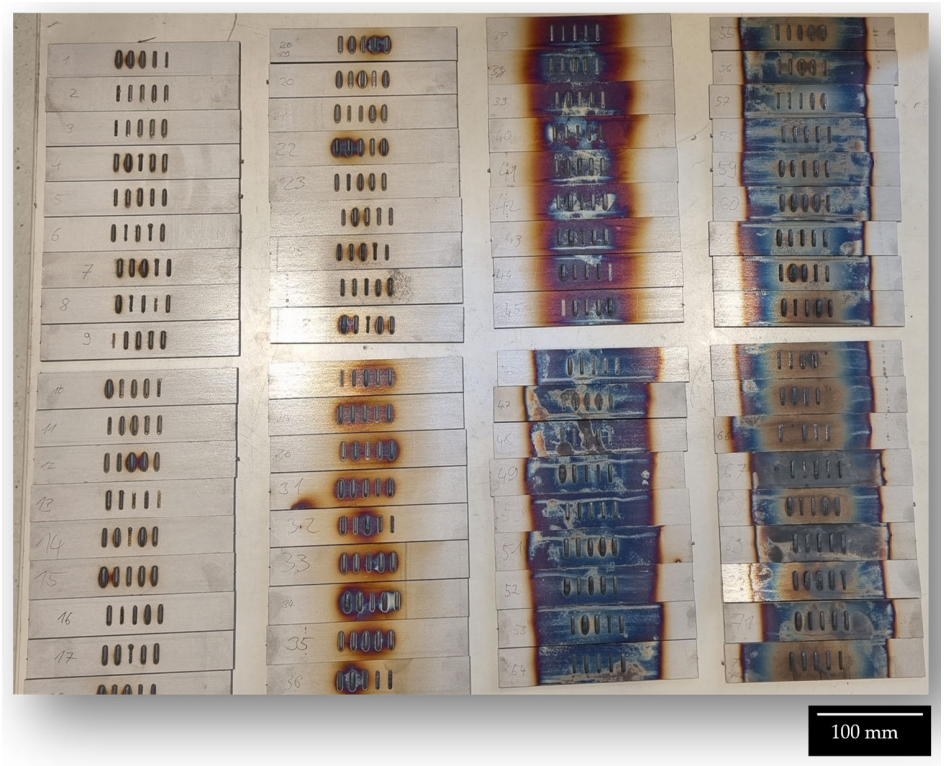

Figure 3. Produced samples sorted in ascending bins by substrate temperature in a zig-zag-fashion (start: upper left corner → down → right and up).

3. Results and Discussion

To study the process parameter influence, each bead track was cut, polished, and etched using V2A etching solution. Cross-sectional images were captured using the VHX5000 digital microscope at 200× magnification to measure the bead height, width, dilution, and contact angle. Image analysis and measurements were conducted using Keyence software (Version 1.8.04) to ensure precision in data collection. It should be noted that there can be potential measurement errors from the Keyence VHX5000 digital microscope (KEYENCE DEUTSCHLAND GmbH, Neu-Isenburg, Germany) due to factors, such as magnification variability, calibration inaccuracies, parallax error, user-dependent variability, and environmental influences. These errors could introduce deviations of up to a few micrometers, potentially impacting the precision of bead geometry predictions; however, as the same instrument and settings are consistently applied to all samples, any measurement deviations are likely uniform, ensuring consistent accuracy across the dataset. The data collected were used to create a regression model to predict the machine settings needed to achieve specific bead characteristics. Key measurements included the bead width (b), bead height (a), dilution, and contact angle (e). The contact angle was measured on both sides of the bead and averaged. The dilution was calculated as the ratio of the molten substrate area (d) to the total molten area (c + d), using Equation (1) as shown in Figure 4. Regression analysis was performed using Minitab 2022 with boundary conditions listed in Table 4. The contact angle was used to ensure that it remained above 90° to reduce the risk of fusion defects. Although powder mass flow could not be controlled directly, it was used as a predictor in the model to help calculate the required laser power and traverse speed for a given powder mass flow and substrate temperature to achieve the desired bead geometry.

$$\text{Dilution} = \frac{\text{Area within substrate(d)}}{\text{Total molten area } (c + d)} \quad (1)$$

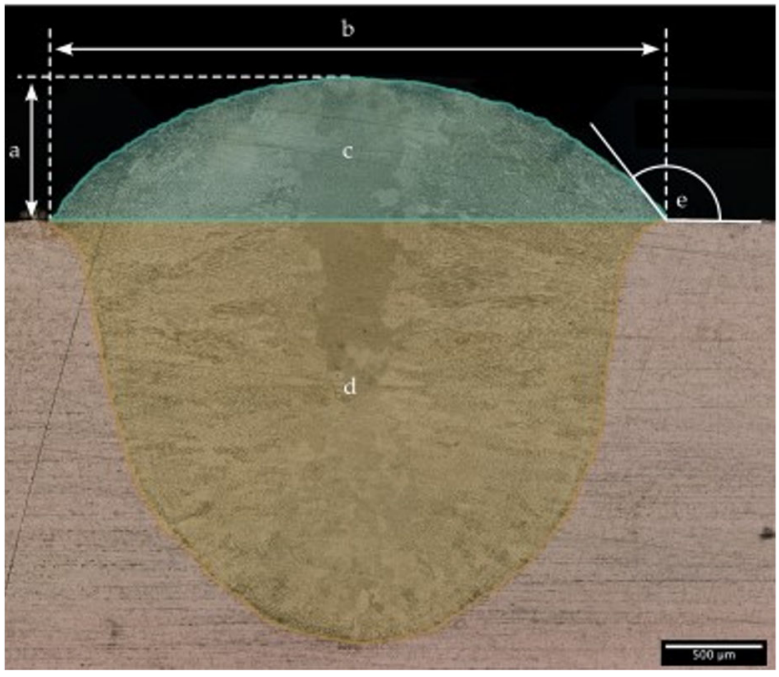

Figure 4. Cross-sectional image of a bead track with the measured geometric characteristics. a: Height, b: width, c: beaded-on area above substrate surface, d: beaded-in area within substrate, e: contact area.

Building on the initial linear regression model, further analysis using quadratic regression was carried out to account for non-linear effects between the process parameters and bead characteristics. This advanced modeling approach allowed us to capture the complex interactions between key variables, such as the bead width, bead height, dilution, substrate temperature, and powder mass flow. The inclusion of quadratic terms helped to better explain the non-linear relationships observed in the data, where the effects of certain parameters exhibited diminishing or accelerating trends at higher levels.

Table 4. Boundary conditions used to generate the regression equation via Minitab 2018.

Responses	Predictors
■ Feed rate	■ Bead width
■ Laser power	■ Bead height
■ Contact angle	■ Dilution
	■ Substrate temperature
	■ Powder mass flow

For the feed rate, the quadratic regression model provided a more accurate representation of how the process variables interact. The model Equation (2) reveals that the powder mass flow and dilution have significant non-linear effects on the feed rate, with positive linear effects that taper off at higher values, as indicated by the negative quadratic terms. Despite showing significant effects in the quadratic model, the Pearson correlation analysis indicated no direct linear relationship between the powder mass flow or substrate temperature and the feed rate, as both had a Pearson correlation coefficient of zero (Table 5). The quadratic terms, however, demonstrated the complex interplay between the bead height and dilution, suggesting optimal ranges for minimizing defects while maintaining the desired feed rate.

Table 5. Correlation matrix derived using Pearson correlation coefficient containing the *p*-value with respect to parameters.

Response	Bead Width	Bead Height	Dilution	Substrate Temperature	Powder Mass Flow
Feed rate	−0.225	−0.597	0.026	0.000	0.000
Contact Angle	−0.278	0.610	−0.613	−0.336	0.566
Laser Power	0.527	0.103	0.638	0.000	0.000

As shown in Equation (3), the influence of the dilution was significant, with strong linear and non-linear effects. The quadratic term for the powder mass flow in the model suggested a diminishing effect, but the Pearson correlation analysis revealed no direct linear relationship between the powder mass flow or substrate temperature and laser power, with both having a Pearson correlation coefficient of zero. This indicates that while these variables showed non-linear effects in the model, they are not strong linear predictors of laser power. The analysis instead highlights dilution as a critical factor in determining the required energy input, emphasizing the need for precise control over material deposition to optimize energy consumption during the deposition process. Similarly, for the contact angle, the quadratic model highlights the importance of controlling the bead width, bead height, and dilution to maintain stable bead geometries. The regression model Equation (4) indicated that the dilution had a significant non-linear effect, with increasing values initially reducing the contact angle but eventually reaching a plateau. The Pearson correlation analysis further supported this finding, with the powder mass flow showing the highest

correlation with contact angle stability. In contrast, the bead height had no measurable influence on the contact angle, as indicated by a Pearson correlation coefficient of zero. The inclusion of quadratic terms allowed the model to better predict when the contact angle would fall below critical thresholds, ensuring sufficient fusion between the bead layers. Finally, the quadratic regression model for laser power provided insight into the required energy input based on process parameters.

$$\begin{aligned}\text{Feed rate} = 1029 \quad & -0.0686\ \text{Bead Width} - 1.591\ \text{Bead Height} + 6.69\ \text{Dilution} \\ & -0.272\ \text{Substrate Temperature} + 104.5\ \text{Powder Mass Flow} + 0.000010\ \text{Bead Width}^2 \\ & +0.000357\ \text{Bead height}^2 - 0.0695\ \text{Dilution}^2 + 0.000180\ \text{Substrate Temperature}^2 \\ & -2.126\ \text{Powder Mass Flow}^2\end{aligned} \tag{2}$$

$$\begin{aligned}\text{Laser power} = 144 \quad & -0.112\ \text{Bead Width} + 0.204\ \text{Bead Height} + 5.62\ \text{Dilution} \\ & -1.500\ \text{Substrate Temperature} + 99.6\ \text{Powder Mass Flow} + 0.000117\ \text{Bead Width}^2 \\ & -0.000173\ \text{Bead height}^2 + 0.1405\ \text{Dilution}^2 + 0.000523\ \text{Substrate Temperature}^2 \\ & -2.230\ \text{Powder Mass Flow}^2\end{aligned} \tag{3}$$

$$\begin{aligned}\text{Contact angle} = 88.4 \quad & -0.0362\ \text{Bead Width} + 0.1033\ \text{Bead Height} - 0.666\ \text{Dilution} \\ & -0.0317\ \text{Substrate Temperature} + 4.02\ \text{Powder Mass Flow} + 0.000004\ \text{Bead Width}^2 \\ & -0.000027\ \text{Bead height}^2 + 0.00632\ \text{Dilution}^2 + 0.000001\ \text{Substrate Temperature}^2 \\ & -0.0769\ \text{Powder Mass Flow}^2\end{aligned} \tag{4}$$

The quadratic regression models developed for the feed rate, contact angle, and laser power highlight the complex interactions between the process parameters. The influence of the substrate temperature on bead geometry was investigated. The relationship between the heat input and substrate temperature is essential, as the substrate temperature affects the cooling rate and thermal gradients, impacting heat input stability and, consequently, bead geometry. This relationship is fundamental for understanding how the substrate temperature influences cladding characteristics. The substrate temperature has a clear influence on key bead characteristics, as demonstrated in Figure 5. The graphs highlight the relationship between the substrate temperature and the bead width, contact angle, bead height, and dilution. As seen in Figure 5a, the bead width shows a slight positive linear trend with an increasing substrate temperature. Higher temperatures tend to increase the fluidity (decrease viscosity) of the molten material, allowing it to spread more widely across the substrate, resulting in a gradual increase in the bead width. In contrast, Figure 5b illustrates that the contact angle decreases with an increasing substrate temperature. As the substrate temperature rises, the molten material wets the surface more effectively, resulting in a smaller contact angle. This behavior is beneficial for achieving strong bonding between layers, as lower contact angles generally lead to better fusion. However, the bead height, as shown in Figure 5c, appears to remain relatively constant across varying substrate temperatures, likely due to dominant factors, such as the laser power and powder flow, which more directly control the deposition volume. The substrate temperature mainly affects cooling and solidification rates, with a lesser impact on the bead height. The dilution, presented in Figure 5d, increases with the substrate temperature. Higher temperatures promote the melting of more substrate material, leading to stronger substrate material mixing into the bead pool. This increased dilution enhances bonding but must be controlled to avoid unwanted changes in the microstructure of the bead. In some cases, increased substrate temperatures can alter material wetting behavior and cooling rates, resulting in deviations from predicted values, particularly for the bead width and contact angle. These trends observed in the regression analysis are well captured by the quadratic regression model, which accounts for both linear and non-linear effects of the substrate temperature. Given the importance of the substrate temperature on key bead characteristics, we designed a series of validation experiments to confirm the predictive capability of the regression models

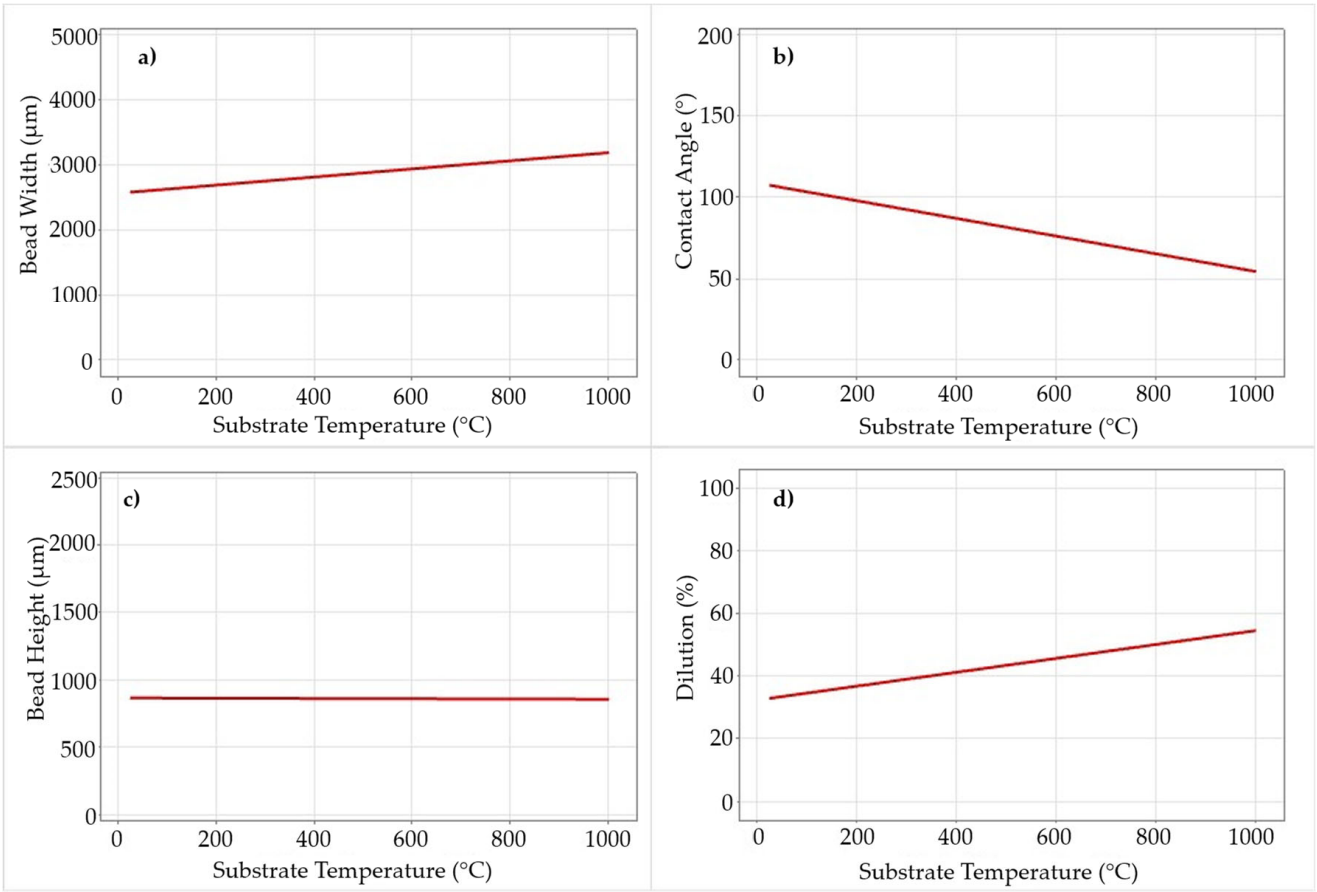

Figure 5. The influence of substrate temperature on key bead characteristics, including the (**a**) bead width, (**b**) contact angle, (**c**) bead height, and (**d**) dilution.

Table 6. Parameters used for desired bead geometry to validate the regression equation.

Substrate Temperature (°C)	Feed rate (mm/min)	Laser Power (W)	Contact Angle (°)
200	764.00	1408.17	112.95
400	751.02	1228.00	106.94
600	752.45	1089.66	101.05
800	768.30	993.16	95.27

To assess the predictive accuracy of the regression models, the target bead geometry dimensions were inputted into the regression equations to calculate the required process parameters, as shown in Table 6. The selected target values were 3 mm for the bead width, 1 mm for the bead height, 15% for the dilution, and 15 g/min for the powder mass flow, with substrate temperatures set at room temperature 200 °C, 400 °C, 600 °C, and 800 °C. For each parameter set, three beads were produced using the same experimental setup as described previously to validate the model. The process parameters—primarily the substrate temperature, laser power, feed rate, and powder mass flow—were systematically varied (within 5% of calculated values), and the actual measured results were compared to the predicted values obtained from the regression models, as shown in Figures 6 and 7.

The experimental results for the bead height, bead width, contact angle, and dilution were compared with the desired target values across substrate temperatures of 200 °C, 400 °C, 600 °C, and 800 °C. Overall, the model was able to predict the bead height, bead width, and contact angle with reasonable accuracy, while it struggled to accurately predict the dilution. For the bead height, the target value was set at 1000 μm, and the experimental

values were slightly lower, with the largest deviation occurring at 200 °C and 400 °C, where the bead height was 886 µm, representing a 11.8% decrease from the target. At the highest substrate temperature of 800 °C, the bead height was 895 µm, a 10.5% decrease, indicating that the model performed relatively well across all temperature ranges. The desired bead width of 3000 µm was also generally achieved, with the largest deviation observed at 400 °C, where the bead width was 2790 µm, a 7% decrease. At 800 °C, the bead width was 2895 µm, a 5% decrease from the desired value. The contact angle predictions were similarly close to the experimental values, with the largest deviation occurring at 800 °C, where the experimental contact angle was 95°, a 25% decrease compared to the predicted value of 127°. At lower temperatures, the deviations were smaller, with the experimental contact angle at 200 °C showing only a 1% decrease. This suggests that while the model remains accurate at lower temperatures, its prediction for the contact angle at higher temperatures requires refinement. However, the model significantly underperformed when predicting the dilution. While the target dilution was set at 15% for all temperatures, the experimental dilution consistently fell short. The largest deviation occurred at 400 °C, where the experimental dilution was 2.6%, representing an 82.7% decrease. At 800 °C, the dilution was only 4.8%, a 68% decrease. This significant deviation underscores the need for further refinement of the model when predicting the dilution, as it is a key parameter in determining the quality of the bead. These results indicate that while the model was effective in predicting the bead height, bead width, and contact angle, it failed to accurately predict the dilution, highlighting the need for further refinement in the process model.

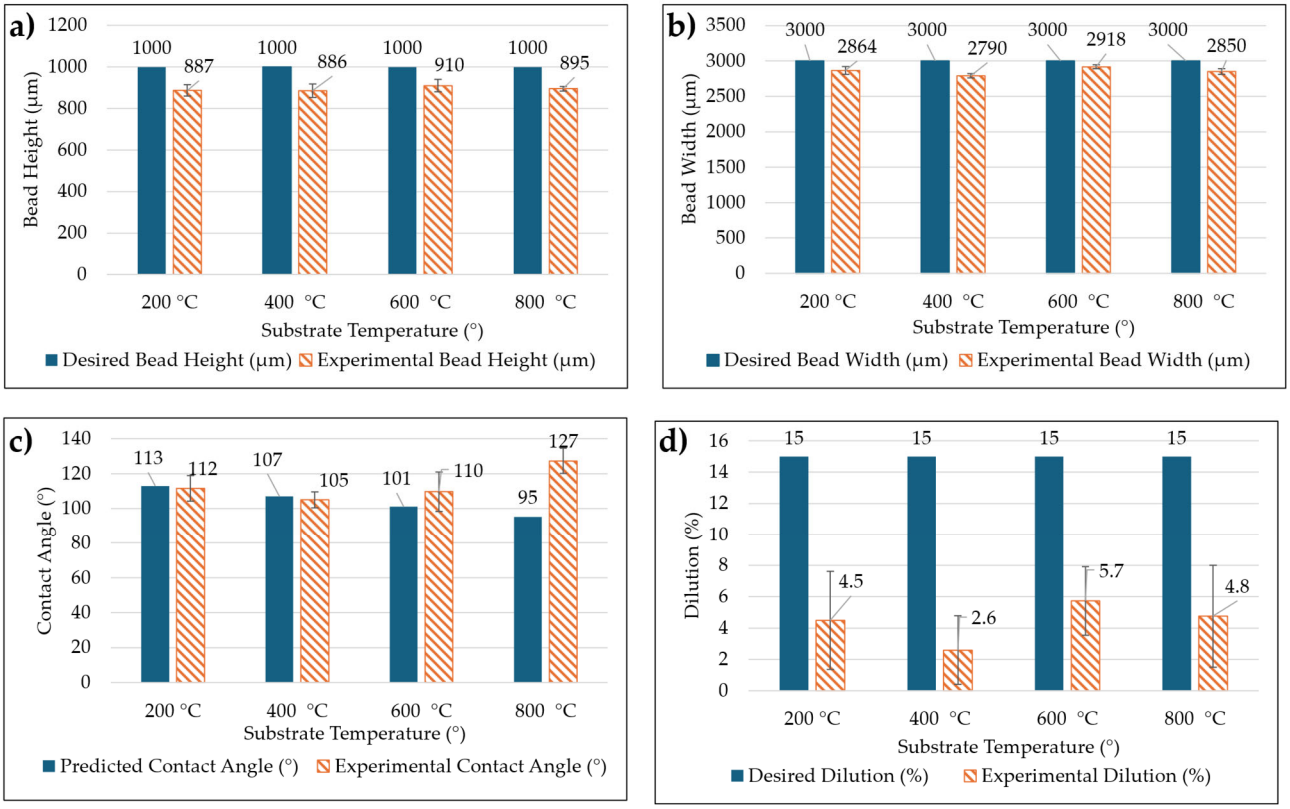

Figure 6. Comparison between the desired and experimental bead characteristics at substrate temperatures of 200 °C, 400 °C, 600 °C, and 800 °C. (**a**) Bead width, (**b**) bead height, (**c**) contact angle, and (**d**) dilution.

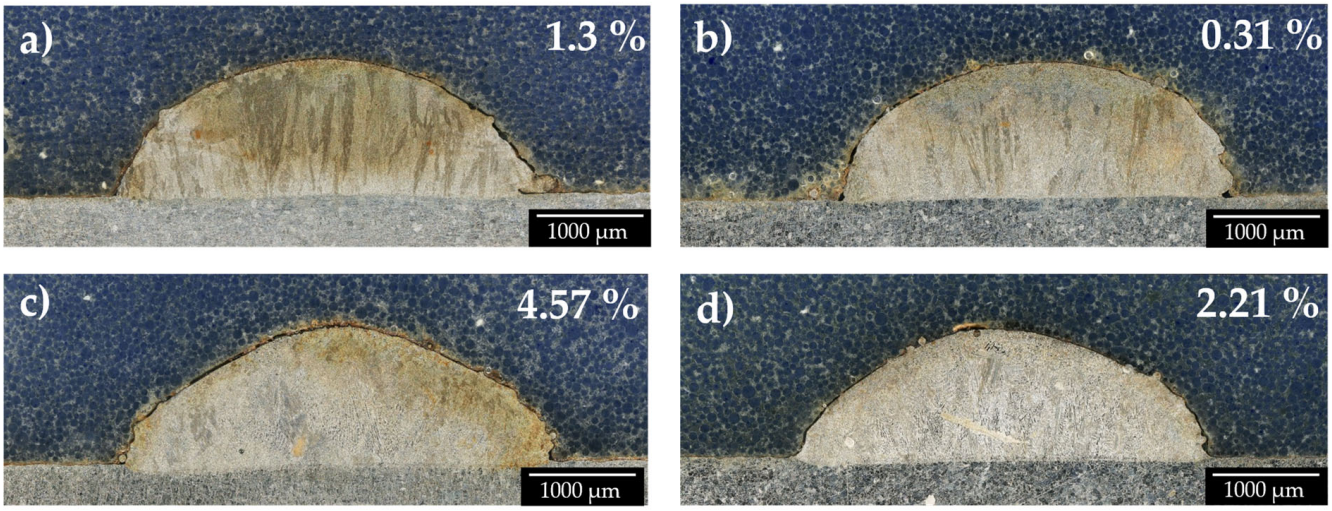

Figure 7. Images of cross-sectional cut beads, with dilution in % in the upper part of pictures, at substrate temperatures of (**a**) 200 °C, (**b**) 400 °C, (**c**) 600 °C, and (**d**) 800 °C.

4. Conclusions

This study investigated the influence of the substrate temperature on bead track geometry in Directed Energy Deposition (DED) processes, with a focus on 316L stainless steel. Using regression models, including both linear and quadratic approaches, we explored how key process parameters, such as the bead width, bead height, contact angle, and dilution, are affected by varying substrate temperatures. The results demonstrated that the developed models were largely successful in predicting the bead height, bead width, and contact angle, with deviations from the desired values generally falling within acceptable ranges. Specifically, the bead width and height showed only minor deviations across the range of substrate temperatures, and the model provided strong predictions for these parameters. The bead height, however, was minimally affected by the substrate temperature, as shown in our results, indicating that factors, such as laser power and powder flow, play a more dominant role in controlling this characteristic. Similarly, contact angle predictions were accurate for lower substrate temperatures, although the model struggled slightly at higher temperatures.

However, the model underperformed in predicting the dilution, with significant deviations from the target values observed at all substrate temperatures. For example, the largest error for dilution occurred at 400 °C, with an experimental value of 2.6%, representing an 82.7% decrease from the target dilution of 15%. This suggests that while the regression models are effective for predicting certain geometric features, the dilution remains a challenging parameter to model accurately. Further refinement of the model and a deeper investigation into the influence of other factors, such as material properties and thermal gradients, will be necessary to improve the accuracy of dilution predictions.

Overall, this study highlights the potential for optimizing DED process parameters through predictive modeling. The insights gained from this work provide a foundation for future efforts to refine the regression models and further improve the accuracy of predictions for all key bead characteristics. Future work will aim to address the challenges in modeling dilution and explore additional process variables to enhance the robustness and reliability of the predictive models for DED applications.

Author Contributions: Conceptualization, S.G., D.L. and T.T.; Methodology, S.G.; Software, D.C.J. and S.G.; Validation, S.G., A.W. and R.R.; Formal analysis, D.C.J. and S.G.; Investigation, S.G., A.W. and R.R.; Resources, T.T.; Data curation, D.C.J. and S.G.; Writing—original draft, D.C.J. and S.G.; Writing—review and editing, D.C.J. and D.L.; Visualization, D.C.J. and S.G.; Supervision, T.T.; Project administration, T.T.; Funding acquisition, T.T. All authors have read and agreed to the published version of the manuscript.

Funding: The article publishing charges were paid for by the University of Paderborn. The DED machine (LT65) used for this research was funded by the Deutsche Forschungsgemeinschaft DFG (No. 428364048).

Data Availability Statement: The original contributions presented in the study are included in the article, further inquiries can be directed to the corresponding author.

Acknowledgments: The authors would like to extend their gratitude to the laboratory technicians of the LiA Chair for their invaluable assistance.

Conflicts of Interest: The authors declare no conflicts of interest.

References

1. Lu, B.; Li, D.; Tian, X. Development Trends in Additive Manufacturing and 3D Printing. *Engineering* **2015**, *1*, 085–089. [CrossRef]
2. Ye, Z.; Zhu, J.; Li, Q.; Mo, B.; Lei, B.; Li, Y.; Wang, C.; Huang, C. A novel method of reliability-centered process optimization for additive manufacturing. *Microelectron. Reliab.* **2018**, *88–90*, 1151–1156. [CrossRef]
3. Bhatia, A.; Sehgal, A.K. Additive manufacturing materials, methods and applications: A review. *Mater. Proc.* **2023**, *81*, 1060–1067. [CrossRef]
4. Ngo, T.D.; Kashani, A.; Imbalzano, G.; Nguyen, K.T.; Hui, D. Additive manufacturing (3D printing): A review of materials, methods, applications and challenges. *Compos. Part B Eng.* **2018**, *143*, 172–196. [CrossRef]
5. Dass, A.; Moridi, A. State of the Art in Directed Energy Deposition: From Additive Manufacturing to Materials Design. *Coatings* **2019**, *9*, 418. [CrossRef]
6. Ahn, D.G. Directed Energy Deposition (DED) Process: State of the Art. *Int. J. Precis. Eng. Manuf. -Green Technol.* **2021**, *8*, 703–742. [CrossRef]
7. Saboori, A.; Aversa, A.; Marchese, G.; Biamino, S.; Lombardi, M.; Fino, P. Application of Directed Energy Deposition-Based Additive Manufacturing in Repair. *Appl. Sci.* **2019**, *9*, 3316. [CrossRef]
8. Bennett, J.L.; Garcia, D.J.; Kendrick, M.; Hartman, T.; Hyatt, G.; Ehmann, K.; You, F.; Cao, J. Repairing Automotive Dies with Directed Energy Deposition: Industrial Application and Life Cycle Analysis. *J. Manuf. Sci. Eng.* **2019**, *141*, 021019. [CrossRef]
9. Aprilia, A.; Wu, N.; Zhou, W. Repair and restoration of engineering components by laser directed energy deposition. *Mater. Today Proc.* **2022**, *70*, 206–211. [CrossRef]
10. Heilemann, M.; Jothi Prakash, V.; Beulting, L.; Emmelmann, C. Effect of heat accumulation on the single track for-mation during laser metal deposition and development of a framework for analyzing new process strategies. *J. Laser Appl.* **2021**, *33*, 012003. [CrossRef]
11. Isquierdo, D.; Siqueira, R.; Carvalho, S.; Lima, M. Effect of the initial substrate temperature on heat transfer and related phenomena in austenitic stainless steel parts fabricated by additive manufacturing using direct energy deposition. *J. Mater. Res. Technol.* **2022**, *18*, 5267–5279. [CrossRef]
12. Moheimani, S.K.; Iuliano, L.; Saboori, A. The role of substrate preheating on the microstructure, roughness, and mechanical performance of AISI 316L produced by directed energy deposition additive manufacturing. *Int. J. Adv. Manuf. Technol.* **2022**, *119*, 7159–7174. [CrossRef]
13. Mani, M.; Lane, B.M.; Donmez, M.A.; Feng, S.C.; Moylan, S.P. A review on measurement science needs for real-time control of additive manufacturing metal powder bed fusion processes. *Int. J. Prod. Res.* **2017**, *55*, 1400–1418. [CrossRef]
14. Aleksandr, K.; Ferdinando, S.; Joel, R.; Joel, C.; Jordan, M.; Thomas, J. Effect of direct energy deposition parameters on morphology, residual stresses, density, and microstructure of 1.2709 maraging steel. *Int. J. Adv. Manuf. Technol.* **2021**, *117*, 1281–1301. [CrossRef]
15. Sreekanth, S.; Ghassemali, E.; Hurtig, K.; Joshi, S.; Andersson, J. Effect of Direct Energy Deposition Process Parameters on Single-Track Deposits of Alloy 718. *Metals* **2020**, *10*, 96. [CrossRef]
16. Mahamood, R.M. Effect of Laser Power and Gas Flow Rate on Properties of Directed Energy Deposition of Titanium Alloy. *Lasers Manuf. Mater. Process.* **2018**, *5*, 42–52. [CrossRef]
17. Koukolíková, M.; Simson, T.; Rzepa, S.; Brázda, M.; Džugan, J. The influence of laser power on the interfaces of functionally graded materials fabricated by powder-based directed energy deposition. *J. Mater. Sci.* **2022**, *57*, 13695–13723. [CrossRef]
18. Kim, T.G.; Shim, D.S. Effect of laser power and powder feed rate on interfacial crack and mechanical/microstructural characteri-zations in repairing of 630 stainless steel using direct energy deposition. *Mater. Sci. Eng. A* **2021**, *828*, 142004. [CrossRef]
19. Borovkov, H.; Yedra, A.G.; Zurutuza, X.; Angulo, X.; Alvarez, P.; Pereira, J.C.; Cortes, F. In-Line Height Meas-urement Technique for Directed Energy Deposition Processes. *J. Manuf. Mater. Process.* **2021**, *5*, 85. [CrossRef]
20. Javidrad, H.; Aydin, H.; Karakaş, B.; Alptekin, S.; Kahraman, A.S.; Koc, B. Process parameter optimization for laser powder directed energy deposition of Inconel 738LC. *Opt. Laser Technol.* **2024**, *176*, 110940. [CrossRef]
21. Zhong, C.; Biermann, T.; Gasser, A.; Poprawe, R. Experimental study of effects of main process parameters on porosity, track geometry, deposition rate, and powder efficiency for high deposition rate laser metal deposition. *J. Laser Appl.* **2015**, *27*, 042003. [CrossRef]
22. Pereira, R.J.R.; de Almeida, F.A.; Gomes, G.F. A multiobjective optimization parameters applied to additive manufacturing: DOE-based approach to 3D printing. *Structures* **2023**, *55*, 1710–1731. [CrossRef]

23. Sciammarella, F.M.; Najafabadi, B.S. Processing Parameter DOE for 316L Using Directed Energy Deposition. *J. Manuf. Mater. Process.* **2018**, *2*, 61. [CrossRef]
24. Stavropoulos, P.; Foteinopoulos, P. Modelling of additive manufacturing processes: A review and classification. *Manuf. Rev.* **2018**, *5*, 2. [CrossRef]